Machine-learning prediction of superconductivity from high-temperature resistivity in Fe-based compounds

Yuchen Wu, Yiwen Liu, Wanyue Lin, Zohar Nussinov, and Sheng Ran*
Department of Physics, Washington University in St. Louis, St. Louis, Missouri 63130, USA

(Received 20 January 2026; accepted 17 June 2026; published 26 June 2026)

Unconventional superconductivity remains one of the central unsolved problems in quantum materials, and revealing its connection to the normal state is widely believed to be key to uncovering the pairing mechanism. Previous efforts have largely focused on the temperature range immediately above the superconducting transition, where specific scattering channels—such as strange-metal transport—have been identified as sharing a possible microscopic origin with superconductivity. Here, we use machine learning to explore possible correlations between normal-state resistivity and superconductivity in Fe-based compounds. We find that resistivity data in the temperature window of 150–300 K, far above the typical critical temperature (T_c) of this family, can be used to classify whether a compound becomes superconducting. Owing to the limited size of the dataset, the underlying physical origin of this correlation cannot yet be determined. Nevertheless, the results suggest that high-temperature resistivity may contain useful empirical information for superconductivity prediction, motivating larger and more systematic experimental datasets.

DOI: 10.1103/r63k-rfdq

I. INTRODUCTION

Superconductivity emerges from the normal state, inheriting its interactions and collective fluctuations. In conventional superconductors, this connection is clear: The same electron-phonon interactions that dominate normal-state resistivity also provide the pairing mechanism described by BCS theory. In unconventional materials, however, the situation is far more complex: The normal state often departs from a simple Fermi liquid and exhibits anomalous behaviors such as the pseudogap and strange-metal transport [1].

Most prior efforts to uncover the link between the normal state and superconductivity have focused on the narrow temperature window immediately above the superconducting transition. In this regime, short-lived Cooper pairs in the precursor superconducting phase can generate an enhanced conductivity [2–5], whose strength is closely tied to critical temperature (T_c). Likewise, in strange metals, the coefficient of the linear-in-T resistivity has been found to scale with T_c, suggesting that anomalous scattering and superconducting pairing may share a common microscopic origin [6–9]. Yet, these relations remain confined to limited ranges of temperature, doping, and material classes, each tied to a single mechanism. No universal normal-state signature has been identified that reliably predicts the onset of superconductivity.

*Contact author: rans@wustl.edu

Published by the American Physical Society under the terms of the Creative Commons Attribution 4.0 International license. Further distribution of this work must maintain attribution to the author(s) and the published article's title, journal citation, and DOI.

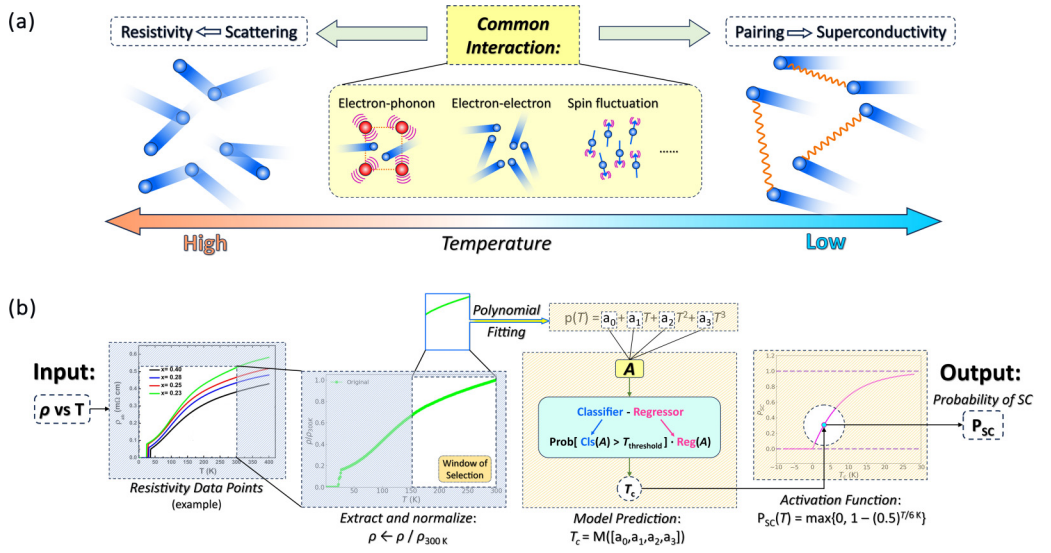

FIG. 1. Schematics of the machine-learning model. (a) The interactions that govern high-temperature resistivity scattering are the same interactions that may drive superconducting pairing at low temperatures. (b) Our machine-learning framework takes polynomial coefficients from high-temperature resistivity fits as input and predicts the superconducting critical temperature T_c. By applying an activation function, the regression models are further converted into classifiers to distinguish superconducting from nonsuperconducting samples.

Here, we examine whether normal-state resistivity well above T_c can provide empirical information about superconductivity. Using machine-learning models trained on resistivity data from Fe-based compounds, we find that high-temperature resistivity contains measurable correlations with whether a compound becomes superconducting, and more weakly with its transition temperature. Because the present dataset is limited in size and contains correlated material series, we do not interpret these correlations as evidence of a universal microscopic signature. Instead, our results establish a data-driven framework for probing how normal-state transport may encode superconducting tendencies.

We focus on Fe-based superconductors for two main reasons. First, their resistivity is intrinsically complex due to the multiband nature and the coexistence of multiple scattering mechanisms, including electron-phonon coupling, electron-electron interactions, and spin fluctuations. While strange-metal behavior has been reported in some cases, it is often intertwined with other scattering effects and therefore less distinct than in cuprates. This richness makes Fe-based superconductors an ideal testing ground, as it avoids bias toward a single interaction channel. Second, these materials have been extensively studied under chemical substitution and applied pressure, providing a large body of resistivity data that spans both superconducting and nonsuperconducting samples with otherwise comparable properties, enabling meaningful comparisons.

II. METHODS

In the high-temperature range, Fe-based compounds are in their paramagnetic states. At low temperatures, they will either remain in the paramagnetic state or enter magnetic ordered state or superconducting state. Our goal is to predict whether it enters the superconducting state, and its transition temperature T_c, using resistivity data in the paramagnetic state in temperature range of ($T_{\min}$, $T_{\max}$), as illustrated in Fig. 1. Our raw dataset consists of temperature-dependent electrical resistivity curves of Fe-based superconductor family, extracted from published figures using online digitization tools. To ensure data quality, we included only resistivity curves measured on

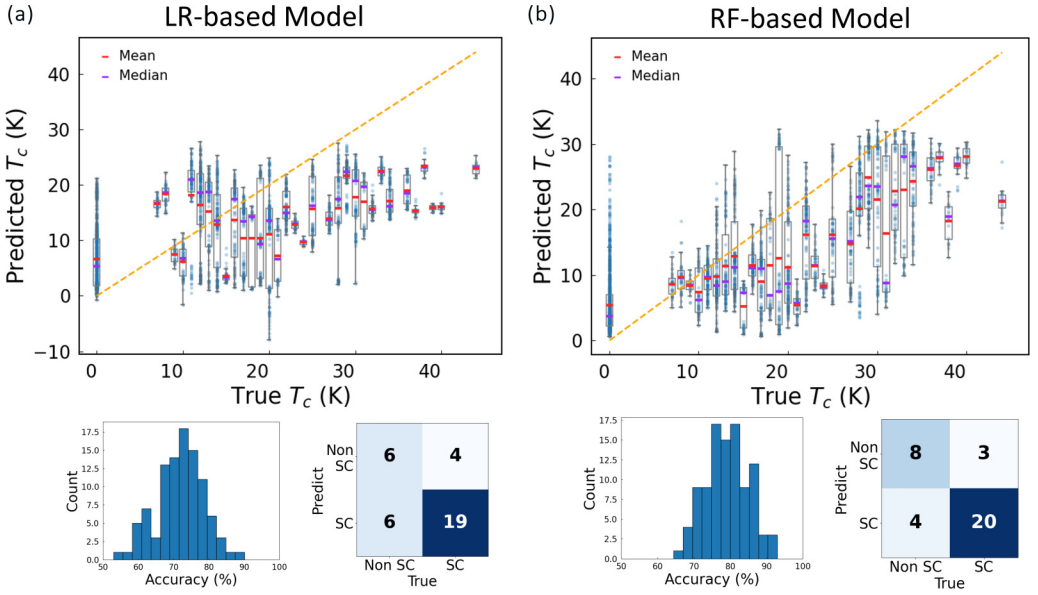

FIG. 2. The performance of the two models on the testing dataset. In each panel, the bigger plot on the top is the predicted T_c plotted against the true T_c of testing data; the labels are the mean and median of predicted T_c (over 100 random splits of training and testing datasets) for each unique value of true T_c. The smaller plot on the bottom left is the distribution of the model's accuracy score over 100 random splits of training and testing datasets. The plot on the bottom right is a snapshot of the confusion matrix of the model. These plots are made for each model: (a) linear regression + logistic regression; (b) random forest regression + random forest classification.

high-quality single crystals or thin films that span a full temperature range from 300 K down to 2 K (or below). In total, 175 datasets were compiled, including 115 superconducting and 60 nonsuperconducting samples [10–31]. Instead of feeding the raw resistivity curves directly into the models, we first fit each dataset with third-order polynomials and use the resulting coefficients as input features (see details in the Supplemental Material [32]). This approach suppresses noise and digitization artifacts, reduces dimensionality of input data, and provides features that are physically interpretable in terms of different scattering contributions. We trained two hybrid regression models consisting of a classifier and a regressor based on linear regression (LR) and random forest (RF).

III. RESULTS

Our main results, obtained with $T_{\min} = 150$ K and $T_{\max} = 300$ K, are summarized in Fig. 2. The predicted transition temperatures (vertical axis) are plotted against the true values (horizontal axis) for 100 runs with random train-test splits, with the diagonal line $y = x$ marking perfect agreement. For nonsuperconducting samples, true values of T_c were set to zero. For each model, we display the mean, median, and the interquartile range containing 75% of the data. To obtain reliable statistics, we evaluated the classification accuracy—defined as the fraction of correct predictions in the test data—over 1000 random splits, and present the resulting histograms for each model along with a representative confusion matrix.

The other performance metrics obtained from 1000 random train-test splits are summarized in Table I for each model: the coefficient of determination R^2, which measures the fraction of variance in the true values explained by the predictions (with 0 indicating no correlation and 1 indicating perfect correlation); the root mean squared error (RMSE), which quantifies the magnitude of the prediction error; the area under the receiver operating characteristic curve (AUROC), which

TABLE I. Comparison of model performance metrics. The coefficient of determination R^2 measures the fraction of variance in the true values explained by the predictions (with 0 indicating no correlation and 1 indicating perfect correlation). The RMSE quantifies the magnitude of the prediction error. The AUROC assesses the ability to discriminate between superconducting and nonsuperconducting samples (with 0.5 indicating no predictive power and 1 indicating perfect discrimination). The accuracy measures the fraction of correct predictions. The sensitivity measures the fraction of true positives correctly identified. The specificity measures the fraction of true negatives correctly identified.

Model	R^2 score	RMSE	AUROC	Accuracy	Std accuracy	Sensitivity	Specificity
LR based	0.22	10.6	0.82	0.73	0.07	0.83	0.55
RF based	0.44	9.1	0.86	0.80	0.06	0.87	0.68

assesses the ability to discriminate between superconducting and nonsuperconducting samples (with 0.5 indicating no predictive power and 1 indicating perfect discrimination); the sensitivity, which measures the fraction of true positives correctly identified; and the specificity, which measures the fraction of true negatives correctly identified.

The LR-based model serves as a baseline, fitting a single linear relation to the data. The predicted T_c values collapse into a narrow range around $\sim$15 K, largely independent of the true T_c, leading to a low R^2 of 0.22, which indicates a weak correlation between predicted and actual transition temperatures. In contrast, the same model achieves a classification accuracy of 73% and an AUROC of 0.82, demonstrating a strong ability to distinguish superconducting from nonsuperconducting samples despite its poor quantitative prediction of T_c.

The RF-based model exhibits improved performance. The predicted T_c values follow the experimental values slightly more closely and align better with the $y = x$ line in Fig. 2, although noticeable scatter remains. This results in an R^2 of 0.44, significantly higher than that of the LR model. Meanwhile, both the classification accuracy and AUROC exceed 0.8, indicating robust classification capability. In both LR and RF models, the classification performance is significantly stronger than the prediction of T_c, which is intrinsically more challenging. The superior performance of the RF model over linear regression suggests that the signatures of superconductivity are encoded in nonlinear combinations of features, rather than in any single linear trend.

To gain more insight into the physical origin of the predictive power of our model, we systematically varied the temperature ranges used for training and monitored both AUROC and R^2 of the RF model, which quantifies the ability to distinguish superconducting from nonsuperconducting samples and to predict T_c, respectively. First, we fixed the upper bound at $T_{\max} = 300$ K and gradually increased the lower bound $T_{\min}$ starting from 150 K. As shown in Fig. 3(a), the AUROC remains approximately constant at around 0.8 and decreases only slightly as $T_{\min}$ increases. In contrast, R^2 drops rapidly, falling to about 0.1 once $T_{\min}$ exceeds 200 K. This indicates that the data in the 200–300 K range carry essentially no predictive information about T_c, even though classification information persists over a broader temperature range extending from roughly 150 to 300 K. Consistently, when we fix $T_{\min} = 150$ K and reduce $T_{\max}$ from 300 to 200 K, the R^2 value varies modestly but stays above 0.3 and the AUROC remains nearly unchanged at approximately 0.85.

To further confirm this trend, we tested sliding temperature windows of fixed width 50 K across the full temperature range. As the window moves toward higher temperatures, the AUROC decreases slightly but consistently remains above 0.7. In contrast, the coefficient of determination R^2 drops rapidly and falls below 0.1 once the lower bound of the window $T_{\min}$ exceeds 200 K. Taken together, these results demonstrate that while the most informative resistivity data for predicting the precise value of T_c are concentrated at lower temperatures, the ability to classify whether a material is superconducting extends over a much broader temperature window, roughly spanning 150–300 K, with a slightly enhanced contribution from the 150–250 K range.

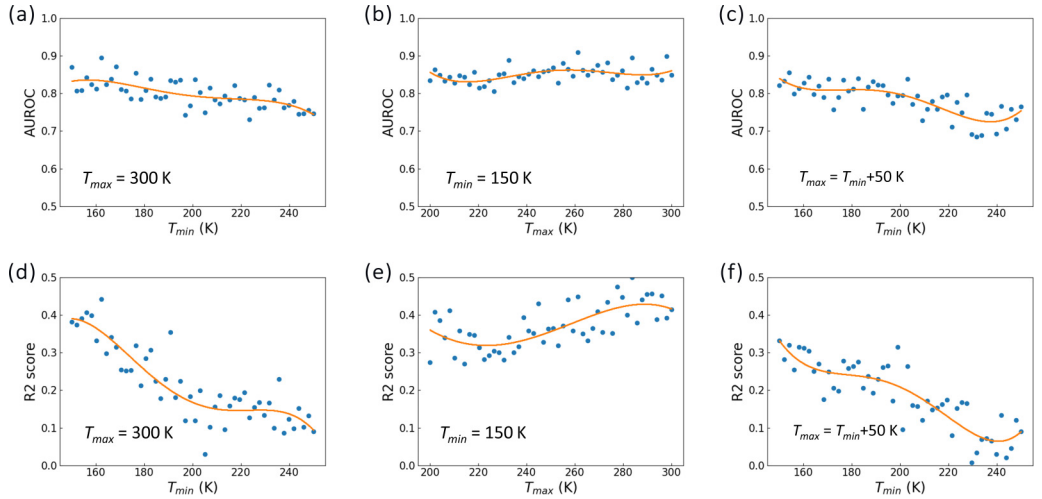

FIG. 3. (a)–(c) The changes in AUROC score with varying range of temperature used by the model. (a) Fix $T_{\max} = 300\,\mathrm{K}$, vary $T_{\min}$; (b) fix $T_{\min} = 150\,\mathrm{K}$, vary $T_{\max}$; and (c) translation of the temperature range with $T_{\max} = T_{\min} + 50\,\mathrm{K}$. (d), (e) The changes in R^2 score with varying range of temperature used by the model. (d) Fix $T_{\max} = 300\,\mathrm{K}$, vary $T_{\min}$; (e) fix $T_{\min} = 150\,\mathrm{K}$, vary $T_{\max}$; and (f) translation of the temperature range with $T_{\max} = T_{\min} + 50\,\mathrm{K}$.

Our results contradict the conventional wisdom in the search for the pairing mechanism of unconventional superconductivity. Prior studies have largely focused on the temperature range immediately above T_c. In some classes of unconventional superconductors, the coefficient of the linear-in-T resistivity—a hallmark of strange-metal transport—has been shown to scale with T_c [6–9]. However, this correlation is confined to a narrow temperature window just above the transition, typically below 100 K [6], beyond which conventional Fermi-liquid behavior reemerges. Precursor effects have also been reported in cuprates: Above T_c, short-lived Cooper pairs can form and break, producing an enhanced conductivity known as paraconductivity [2–5], whose magnitude is closely tied to T_c. Yet, paraconductivity is likewise restricted to a very limited range, usually no more than 20% of T_c [4]. In both cases, the relation holds only for selected materials and centers on a single mechanism. In contrast, our dataset spans multiple Fe-based superconductor families, and our data reveal a strong correlation between superconductivity and the normal-state resistivity in the temperature range of 150–300 K.

We also trained models using selected subsets of polynomial coefficients obtained from the temperature-dependent resistivity fits, as summarized in Table II. Here, the coefficients of the T^0, T^1, T^2, and T^3 terms in the cubic polynomial fits of the normal-state resistivity are referred to as the zeroth-, first-, second-, and third-order terms, respectively. The zeroth-order term plays the least important role: When only this term is used, the AUROC drops from 0.86 to 0.67 and the R^2 value falls to nearly zero. In contrast, the first-order term carries the strongest individual predictive power—Using it alone results in the smallest reduction in both AUROC and R^2. Importantly, however, the relevant information is not exclusively contained in the first-order term. For example, using only the second-order term yields an AUROC only slightly lower than that obtained from the first-order term. Moreover, when the first-order term is excluded, a combination of the zeroth-, second-, and third-order terms achieves better overall performance than using the first-order term alone. Taken together, these results indicate that the correlation with superconductivity is distributed primarily across the first-, second-, and third-order terms, with the first-order contribution being slightly more dominant but not singularly decisive. The selected polynomial coefficients may reflect contributions from different temperature-dependent scattering processes in the normal-state

TABLE II. Performance of models trained with selected polynomial coefficients. The entries indicate which coefficients of the polynomial fit $\rho(T) = a_0 + a_1T + a_2T^2 + a_3T^3$ are included as input features for the model.

Coefficients	R^2 score	RMSE	AUROC	Accuracy	Std accuracy	Sensitivity	Specificity
0, 1, 2, 3	0.44	9.1	0.86	0.80	0.06	0.87	0.68
0	0.06	11.73	0.67	0.64	0.07	0.69	0.54
1	0.17	10.93	0.80	0.70	0.07	0.72	0.69
2	0.10	11.56	0.77	0.73	0.07	0.76	0.67
3	0.05	11.87	0.76	0.75	0.07	0.78	0.70
1, 2, 3	0.37	9.55	0.85	0.81	0.07	0.87	0.68
0, 2, 3	0.33	9.8	0.80	0.73	0.07	0.81	0.59
0, 1, 3	0.40	9.36	0.84	0.78	0.07	0.85	0.65
0, 1, 2	0.42	9.16	0.84	0.79	0.06	0.83	0.71

resistivity. However, these coefficients are empirical descriptors of curve shape and should not be interpreted as direct microscopic scattering channels. Clarifying the physical origin of the observed correlations will require larger, more systematic datasets and complementary theoretical analysis.

One limitation of the current study is the size and composition of the dataset. Ideally, a statistically representative dataset would require samples drawn independently from the full space of Fe-based superconductors, which is practically unattainable. In the absence of a comprehensive public database, we constructed our dataset from the published literature, which inevitably introduces biases toward certain compounds. At the same time, we note that some samples are closely related through doping or pressure tuning. While this may appear to introduce redundancy, such samples often exhibit distinct superconducting behaviors, including different transition temperatures or the absence of superconductivity. Distinguishing between these closely related cases is therefore a nontrivial and physically meaningful task, reflecting genuine predictive capability rather than a trivial consequence of dataset composition.

To reveal the limitation due to the dataset size, we performed additional tests with various conditions applied to the dataset, the results of which are shown in the Supplemental Material [32]. As shown in the row "Leave one family (Ca) out (32 data)," we selected all Ca family compounds as the testing set and train the model exclusively on the rest 143 data. The AUROC drops remain around 0.8, while the R^2 value falls to nearly zero. This implies that the model trained on Ca-exclusive data has limited prediction power on the Ca family; thus, the related samples from the same family may have indeed inflated the performance. In the next trial, we trained and tested the model on the largest Ba family in our dataset, consisting of 56 superconducting samples among 106 total samples. As the data are from a common family, the model can no longer be learning cross-family relations in the dataset. The model reaches 0.52 R^2 score, comparable classification accuracy, and more balanced specificity and sensitivity compared to the original model. This is clear evidence that within the Ba family, the signal of superconductivity lies in normal-state resistivity. Next, we selected all compounds from one published paper as testing dataset, which consists of the series of compounds $Ba(Fe_xRu_{1-x})_2As_2$ with various doping levels and various pressures with different types of pressure cells. There are 31 data in total in the testing dataset, and the model is trained on the rest of all data. As shown in the row "Leave one series/paper out (31 data)," the model results in 0.16 R^2 score, 0.83 classification accuracy, 0.92 sensitivity, and 0.60 specificity. These metrics lies between the original model (as shown in the first row of the table) and the leave-one-family trial, indicating that the model has better generalized predictive power across series/papers, compared to its predictive power across material families. Overall, these grouped validation trials, together with the averaged metrics from random train-test splits, indicate that the model captures meaningful correlations within related material families or series. However, its performance degrades substantially when applied to an unseen family, suggesting that the present dataset does not yet support robust family-independent prediction. Thus, our current results should be interpreted as evidence for within-family predictive

correlations in high-temperature resistivity, rather than as a universal superconductivity signature across Fe-based compounds.

Next, in polynomial-fitting tests, we compared model performance using different polynomial degrees for feature extraction. These tests show that third-, fourth-, and fifth-degree polynomials provide the most appropriate empirical representations for our dataset: First- and second-degree polynomials underfit the resistivity curves and lead to reduced test scores, whereas sixth-degree polynomials begin to overfit and introduce a bias toward classifying samples as superconducting. We also performed additional baseline tests using a simple slope-based predictor, a regression-only model, and permutation of the target labels. These tests show that the full model performs better than trivial or purely probabilistic predictions. At the same time, they also reveal important limitations: The superconducting-only regression remains weak, and the simple slope baseline already captures a substantial fraction of the classification performance. The limitations of the dataset remain the major drawback of the study. Because truly random sampling from the full space of Fe-based compounds is not practically possible, and because the available data must be assembled manually from the published literature, the dataset is inevitably small, heterogeneous, and biased toward certain material families and series. Nevertheless, these validation tests provide a useful assessment of what the model can and cannot support, and motivate larger, more systematic experimental datasets for future studies.

IV. CONCLUSION

To conclude, our study explores whether high-temperature normal-state resistivity can be used to predict superconductivity in Fe-based compounds. We find that resistivity data well above T_c contain empirical information that enables classification of superconducting and nonsuperconducting samples within the compiled dataset, although the prediction of the precise transition temperature remains more limited. The validation tests further show that this predictive capability is strongest within related material families or series, while generalization to unseen families remains challenging. More broadly, our work demonstrates a data-driven framework for using experimental transport curves, rather than chemical composition alone [33–45], to study superconductivity and other quantum materials. This approach is more directly connected to physical observables, but it is currently limited by the small, heterogeneous, and manually assembled nature of the dataset. Larger and more systematically curated databases of experimental physical properties will be essential for achieving robust, family-independent predictions and for clarifying the underlying physics.

ACKNOWLEDGMENTS

We acknowledge fruitful discussions with Shaffique Adam, Tao Ju, and Daoyi Zhu. The work at Washington University was supported by the National Science Foundation (NSF) Division of Materials Research Award No. DMR-2512965.

DATA AVAILABILITY

The data that support the findings of this article are not publicly available upon publication because it is not technically feasible and/or the cost of preparing, depositing, and hosting the data would be prohibitive within the terms of this research project. The data are available from the authors upon reasonable request.

[1] B. Keimer, S. A. Kivelson, M. R. Norman, S. Uchida, and J. Zaanen, From quantum matter to high-temperature superconductivity in copper oxides, Nature (London) **518**, 179 (2015).

[2] E. Silva, S. Sarti, R. Fastampa, and M. Giura, Excess conductivity of overdoped $Bi_2Sr_2CaCu_2O_{8+x}$ crystals well above T_c, Phys. Rev. B **64**, 144508 (2001).
[3] D. Pelc, M. Vuckovic, M. S. Grbić, M. Požek, G. Yu, T. Sasagawa, M. Greven, and N. Barišić, Emergence of superconductivity in the cuprates via a universal percolation process, Nat. Commun. **9**, 4327 (2018).
[4] P. Popčević, D. Pelc, Y. Tang, K. Velebit, Z. Anderson, V. Nagarajan, G. Yu, M. Požek, N. Barišić, and M. Greven, Percolative nature of the direct-current paraconductivity in cuprate superconductors, npj Quantum Mater. **3**, 42 (2018).
[5] G. Yu, D.-D. Xia, D. Pelc, R.-H. He, N.-H. Kaneko, T. Sasagawa, Y. Li, X. Zhao, N. Barišić, A. Shekhter, and M. Greven, Universal precursor of superconductivity in the cuprates, Phys. Rev. B **99**, 214502 (2019).
[6] J. Yuan *et al.*, Scaling of the strange-metal scattering in unconventional superconductors, Nature (London) **602**, 431 (2022).
[7] R. L. Greene, P. R. Mandal, N. R. Poniatowski, and T. Sarkar, The strange metal state of the electron-doped cuprates, Annu. Rev. Condens. Matter Phys. **11**, 213 (2020).
[8] C. M. Varma, *Colloquium:* Linear in temperature resistivity and associated mysteries including high temperature superconductivity, Rev. Mod. Phys. **92**, 031001 (2020).
[9] X. Jiang *et al.*, Interplay between superconductivity and the strange-metal state in FeSe, Nat. Phys. **19**, 365 (2023).
[10] F. Li *et al.*, Bulk superconductivity up to 96 K in pressurized nickelate single crystals, Nature **649**, 871 (2026).
[11] N. Ni, M. E. Tillman, J.-Q. Yan, A. Kracher, S. T. Hannahs, S. L. Bud'ko, and P. C. Canfield, Effects of Co substitution on thermodynamic and transport properties and anisotropic Hc_2 in $Ba(Fe_{1-x}Co_x)_2As_2$ single crystals, Phys. Rev. B **78**, 214515 (2008).
[12] A. Thaler, H. Hodovanets, M. S. Torikachvili, S. Ran, A. Kracher, W. Straszheim, J. Q. Yan, E. Mun, and P. C. Canfield, Physical and magnetic properties of $Ba(Fe_{1-x}Mn_x)_2As_2$ single crystals, Phys. Rev. B **84**, 144528 (2011).
[13] N. Ni, A. Thaler, J. Q. Yan, A. Kracher, E. Colombier, S. L. Bud'ko, P. C. Canfield, and S. T. Hannahs, Temperature versus doping phase diagrams for $Ba(Fe_{1-x}TM_x)_2As_2$ (TM = Ni, Cu, Cu/Co) single crystals, Phys. Rev. B **82**, 024519 (2010).
[14] N. Ni, A. Thaler, A. Kracher, J. Q. Yan, S. L. Bud'ko, and P. C. Canfield, Phase diagrams of $Ba(Fe_{1-x}M_x)_2As_2$ single crystals (M = Rh, Pd), Phys. Rev. B **80**, 024511 (2009).
[15] A. Thaler, N. Ni, A. Kracher, J. Q. Yan, S. L. Bud'ko, and P. C. Canfield, Physical and magnetic properties of $Ba(Fe_{1-x}Ru_x)_2As_2$ single crystals, Phys. Rev. B **82**, 014534 (2010).
[16] S. Kasahara, T. Shibauchi, K. Hashimoto, K. Ikada, S. Tonegawa, R. Okazaki, H. Shishido, H. Ikeda, H. Takeya, K. Hirata, T. Terashima, and Y. Matsuda, Evolution from non-Fermi- to Fermi-liquid transport via isovalent doping in $BaFe_2(As_{1-x}P_x)_2$ superconductors, Phys. Rev. B **81**, 184519 (2010).
[17] H. Luo, Z. Wang, H. Yang, P. Cheng, X. Zhu, and H.-H. Wen, Growth and characterization of $A_{1-x}K_xFe_2As_2$ (A = Ba, Sr) single crystals with x = 0–0.4, Supercond. Sci. Technol. **21**, 125014 (2008).
[18] M. S. Torikachvili, S. L. Bud'ko, N. Ni, and P. C. Canfield, Effect of pressure on the structural phase transition and superconductivity in $(Ba_{1-x}K_x)Fe_2As_2$ (x = 0 and 0.45) and $SrFe_2As_2$ single crystals, Phys. Rev. B **78**, 104527 (2008).
[19] Y. Imai, Y. Sawada, F. Nabeshima, D. Asami, M. Kawai, and A. Maeda, Control of structural transition in $FeSe_{1-x}Te_x$ thin films by changing substrate materials, Sci. Rep. **7**, 46653 (2017).
[20] Y. Zhu, D. Peng, E. Zhang, B. Pan, X. Chen, L. Chen, H. Ren, F. Liu, Y. Hao, and N. Li, Superconductivity in pressurized trilayer $La_4Ni_3O_{10-\delta}$ single crystals, Nature (London) **631**, 531 (2024).
[21] K. Kirshenbaum, S. R. Saha, T. Drye, and J. Paglione, Superconductivity and magnetism in platinum-substituted $SrFe_2As_2$ single crystals, Phys. Rev. B **82**, 144518 (2010).
[22] S. Ran, S. L. Bud'ko, W. E. Straszheim, J. Soh, M. G. Kim, A. Kreyssig, A. I. Goldman, and P. C. Canfield, Control of magnetic, nonmagnetic, and superconducting states in annealed $Ca(Fe_{1-x}Co_x)_2As_2$, Phys. Rev. B **85**, 224528 (2012).
[23] S. Ran, S. L. Bud'ko, W. E. Straszheim, and P. C. Canfield, Combined effects of transition metal (Ni and Rh) substitution and annealing/quenching on the physical properties of $CaFe_2As_2$, Phys. Rev. B **90**, 054501 (2014).

[24] M. Xu, J. Schmidt, M. A. Tanatar, R. Prozorov, S. L. Bud'ko, and P. C. Canfield, Superconductivity and magnetic and transport properties of single-crystalline $CaK(Fe_{1-x}Cr_x)_4As_4$, Phys. Rev. B **107**, 134511 (2023).

[25] Q. Hou, L. Sun, Y. Sun, and Z. Shi, Review of single crystal synthesis of 11 iron-based superconductors, Materials **16**, 4895 (2023).

[26] S. K. Kim, M. S. Torikachvili, E. Colombier, A. Thaler, S. L. Bud'ko, and P. C. Canfield, Combined effects of pressure and Ru substitution on $BaFe_2As_2$, Phys. Rev. B **84**, 134525 (2011).

[27] S. K. Kim, E. Colombier, N. Ni, S. L. Bud'ko, and P. C. Canfield, Evolution of the electronic transport properties of V_6O_{11} and V_7O_{13} under pressure, Phys. Rev. B **87**, 115140 (2013).

[28] S. K. Kim, M. S. Torikachvili, S. L. Bud'ko, and P. C. Canfield, Search for pressure-induced quantum criticality in $YbFe_2Zn_{20}$, Phys. Rev. B **88**, 045116 (2013).

[29] Y. Sun, T. Yamada, S. Pyon, and T. Tamegai, Influence of interstitial Fe to the phase diagram of $Fe_{1+y}Te_{1-x}Se_x$ single crystals, Sci. Rep. **6**, 32290 (2016).

[30] E. Sterpetti, J. Biscaras, A. Erb, and A. Shukla, Comprehensive phase diagram of two-dimensional space charge doped $Bi_2Sr_2CaCu_2O_{8+x}$, Nat. Commun. **8**, 2060 (2017).

[31] S. Cai, J. Zhao, N. Ni, J. Guo, R. Yang, P. Wang, J. Han, S. Long, Y. Zhou, Q. Wu, X. Qiu, T. Xiang, R. J. Cava, and L. Sun, The breakdown of both strange metal and superconducting states at a pressure-induced quantum critical point in iron-pnictide superconductors, Nat. Commun. **14**, 3116 (2023).

[32] See Supplemental Material at http://link.aps.org/supplemental/10.1103/r63k-rfdq for information on methods and addititional data.

[33] D. Kaplan, A. Zheng, J. Blawat, R. Jin, R. J. Cava, V. Oudovenko, G. Kotliar, A. M. Sengupta, and W. Xie, Deep learning-based superconductivity prediction and experimental tests, Eur. Phys. J. Plus **140**, 58 (2025).

[34] Q.-X. Wang, X.-F. Yang, R.-G. Shi, Y.-M. Ren, X.-B. Fan, Z. Qin, and J. Chen, Discovery of novel high-T_c superconductors *via* machine learning-based random forest model, Appl. Phys. A **131**, 622 (2025).

[35] S. G. Jung, G. Jung, and J. M. Cole, Machine-learning predictions of critical temperatures from chemical compositions of superconductors, J. Chem. Inf. Model. **64**, 7349 (2024).

[36] T. Konno, H. Kurokawa, F. Nabeshima, Y. Sakishita, R. Ogawa, I. Hosako, and A. Maeda, Deep learning model for finding new superconductors, Phys. Rev. B **103**, 014509 (2021).

[37] H. Gashmard, H. Shakeripour, and M. Alaei, Predicting superconducting transition temperature through advanced machine learning and innovative feature engineering, Sci. Rep. **14**, 3965 (2024).

[38] X. Li, W. Tu, R. Lv, L. Liu, D. Shao, Y. Sun, and W. Lu, Machine learning accelerated search for superconductors in B-C-N based compounds and $R_3Ni_2O_7$-type nickelates, Phys. Rev. B **113**, 054521 (2026).

[39] S. Zeng, Y. Zhao, G. Li, R. Wang, X. Wang, and J. Ni, Atom table convolutional neural networks for an accurate prediction of compounds properties, npj Comput. Mater. **5**, 84 (2019).

[40] K. Hamidieh, A data-driven statistical model for predicting the critical temperature of a superconductor, Comput. Mater. Sci. **154**, 346 (2018).

[41] A. Sanna, T. F. T. Cerqueira, Y.-W. Fang, I. Errea, A. Ludwig, and M. A. L. Marques, Prediction of ambient pressure conventional superconductivity above 80 K in hydride compounds, npj Comput. Mater. **10**, 44 (2024).

[42] M. J. Hutcheon, A. M. Shipley, and R. J. Needs, Predicting novel superconducting hydrides using machine learning approaches, Phys. Rev. B **101**, 144505 (2020).

[43] K. Choudhary and K. Garrity, Designing high-T_c superconductors with BCS-inspired screening, density functional theory, and deep-learning, npj Comput. Mater. **8**, 244 (2022).

[44] S. Adiga and U. V. Waghmare, Accelerating the search for superconductors using machine learning, Comput. Mater. Sci. **263**, 114453 (2026).

[45] C. Broyles, W. Charles, and S. Ran, Structure-driven prediction of magnetic order in uranium compounds, Phys. Rev. Mater. **8**, 114405 (2024).